

Task and Model Agnostic Adversarial Attack on Graph Neural Networks

Kartik Sharma^{1*}, Samidha Verma², Sourav Medya³,
Arnab Bhattacharya⁴, Sayan Ranu²

¹ Georgia Institute of Technology, Atlanta, USA

² Indian Institute of Technology, Delhi, India

³ University of Illinois, Chicago, USA

⁴ Indian Institute of Technology, Kanpur, India

ksartik@gatech.edu, csy207575@iitd.ac.in, medya@uic.edu, sayanranu@iitd.ac.in, arnabb@iitk.ac.in

Abstract

Adversarial attacks on Graph Neural Networks (GNNs) reveal their security vulnerabilities, limiting their adoption in safety-critical applications. However, existing attack strategies rely on the knowledge of either the GNN model being used or the predictive task being attacked. *Is this knowledge necessary?* For example, a graph may be used for multiple downstream tasks unknown to a practical attacker. It is thus important to test the vulnerability of GNNs to adversarial perturbations in a model and task agnostic setting. In this work, we study this problem and show that GNNs remain vulnerable even when the downstream task and model are unknown. The proposed algorithm, TANDIS (**T**argeted **A**ttack via **N**eighborhood **D**istortion) shows that distortion of node neighborhoods is effective in drastically compromising prediction performance. Although neighborhood distortion is an NP-hard problem, TANDIS designs an effective heuristic through a novel combination of *Graph Isomorphism Network with deep Q-learning*. Extensive experiments on real datasets and state-of-the-art models show that, on average, TANDIS is up to 50% more effective than state-of-the-art techniques, while being more than 1000 times faster.

1 Introduction and Related work

Graph neural networks (GNNs) (Hamilton, Ying, and Leskovec 2017; Kipf and Welling 2017; Velickovic et al. 2018; Nishad et al. 2021; Bhattoo, Ranu, and Krishnan 2022), have received much success in structural prediction tasks (Goyal, Jain, and Ranu 2020; Ranjan et al. 2022; Thangamuthu et al. 2022; Jain et al. 2021; Manchanda et al. 2020). Consequently, GNNs have witnessed significant adoption in the industry (Pal et al. 2020; Jain et al. 2019). It is therefore imperative to ensure that GNNs are secure and robust to adversarial attacks. In this work, we investigate this aspect, identify vulnerabilities, and link them to graph properties that potentially hold the solution towards making GNNs more secure.

An attack may occur either during training (*poisoning*) or testing (*evasion*). The attack strategy depends on the extent of information access. In the literature, primarily, three modes of information access has been studied.

1. **White-box attack (WBA):** In a white-box attack (Liu et al. 2019; Wang and Gong 2019; Wu et al. 2019; Xu et al. 2019a), the attacker has access to all information such as model architecture, model parameters and training hyperparameters.
2. **Black-box attack (BBA):** In a black-box attack (Bojchevski and Günnemann 2019; Chang et al. 2020; Chen et al. 2021; Dai et al. 2018; Gupta and Chakraborty 2021; Li et al. 2020; Ma, Ding, and Mei 2020; Ma et al. 2019; Wang et al. 2020), the attacker does not have access to the training model parameters. The attacker can only pose black-box queries on a test sample and get the model output in return (such as a label or score).
3. **Grey-box attack (GBA):** A grey-box attack is a mix of white-box and black-box attacks (Liu et al. 2019; Sun et al. 2020; Wang and Gong 2019; Zügner, Akbarnejad, and Günnemann 2018; Zügner and Günnemann 2019), where the attacker has partial information of the training model. The extent of partial information depends on the particular attack.

In this work, we focus on *targeted black-box, evasion attacks* (Dai et al. 2018). Specifically, we consider an input test graph $\mathcal{G} = (\mathcal{V}, \mathcal{E}, \mathcal{X})$, a target node $t \in \mathcal{V}$ and a budget \mathcal{B} . Our goal is to introduce at most \mathcal{B} edge alterations (additions or deletions) in \mathcal{G} such that the performance of an *unknown* GNN model \mathcal{M} is maximally reduced on node t .

Limitations of Existing Works: Although a black-box attack does not require any information on the model parameters, they operate under three key assumptions:

1. **Task-specific strategy:** Most GNN models are trained for a specific task (e.g., node classification) using an appropriately chosen loss function. Existing techniques for adversarial attacks tailor their strategy towards a specific prediction task under the assumption that this task is known. Hence, they do not generalize to unseen tasks. While this assumption acts as an added layer of security for GNN models, we ask the question: *Is it possible to design task-agnostic adversarial attacks?*
2. **Knowledge of the GNN model:** Although black-box attacks do not need knowledge of the model parameters, they often assume the model type. For example, an attack may be customized for GCN and, therefore, rendered ineffective if the training model switches to Locality-

*Work done as undergraduate thesis at IIT-Delhi

Algorithm	Task	Model	Label
RL-S2V (Dai et al. 2018)		✓	
GF-ATTACK (Chang et al. 2020)	✓		✓
Wang et al. (Wang et al. 2020)		✓	
TANDIS	✓	✓	✓

Table 1: **Characterization of existing targeted, black-box evasion attacks based on agnosticism of the features.**

aware GNNs (You, Ying, and Leskovec 2019; Nishad et al. 2021).

- Label-dependent:** Several BBA algorithms require knowledge of the ground-truth data. As an example, an algorithm may require knowledge of node labels to adversarially attack node classification. These ground truth data is often not available in public domain. For example, Facebook may tag users based on their primary interest area. But this information is proprietary.

Contributions: Table 1 summarizes the limitations in existing algorithms for targeted BBA. In this work, we bridge this gap. Our key contributions are as follows:

- We formulate the problem of *task, model, and label agnostic black-box evasion attacks* on GNNs. The proposed algorithm, TANDIS (**T**argeted **A**ttack via **N**eighborhood **D**ISTortion), shows that such attacks are indeed possible.
- TANDIS exploits the observation that, regardless of the task or the model-type, if the neighborhood of a node can be *distorted*, the downstream prediction task would be affected. Our analysis shows that budget-constrained neighborhood distortion is NP-hard. This computational bottleneck is overcome, by using a *Graph Isomorphism Network* (GIN) to embed neighborhoods and then using *deep Q-learning* (DQN) to explore this combinatorial space in an effective and efficient manner.
- Extensive experiments on real datasets show that, on average, TANDIS is up to 50% more effective than state-of-the-art techniques for BBA evasion attacks and 1000 times faster. More importantly, TANDIS establishes that task and model agnosticism do not impart any additional security to GNNs.

2 Problem Formulation

We denote a graph as $\mathcal{G} = (\mathcal{V}, \mathcal{E}, \mathcal{X})$ where \mathcal{V} is the set of nodes, \mathcal{E} the set of edges, and \mathcal{X} is the set of attribute vectors corresponding to each node $v \in \mathcal{V}$. In this paper, we assume \mathcal{G} to be an undirected graph. Nonetheless, all of the proposed methodologies easily extend to directed graphs. The *distance* $sp(v, u)$ between nodes v and u is measured in the terms of the length of the shortest path from v to u . The k -hop neighborhood of a node v is therefore defined as $\mathcal{N}_{\mathcal{G}}^k(v) = \{u \in \mathcal{V} \mid sp(v, u) \leq k\}$.

The adjacency matrix of graph \mathcal{G} is denoted as $\mathcal{A}_{\mathcal{G}}$. The *distance* between two undirected graphs, $\mathcal{G} = (\mathcal{G}, \mathcal{E}, \mathcal{X})$ and $\mathcal{G}' = (\mathcal{V}, \mathcal{E}', \mathcal{X})$, with the same node set but different edge set, is defined to be half of the L_1 distance between their adjacency matrices: $d(\mathcal{G}, \mathcal{G}') = \|\mathcal{A}_{\mathcal{G}} - \mathcal{A}_{\mathcal{G}'}\|/2$.

Given a GNN model \mathcal{M} , its performance on graph \mathcal{G} to-

wards a particular predictive task is quantified using a *performance metric* $\mathcal{P}_{\mathcal{M}}(\mathcal{G})$:

$$\mathcal{P}_{\mathcal{M}}^*(\mathcal{G}) = f_1(\{\mathcal{P}_{\mathcal{M}}(\mathcal{G}, v) \mid v \in \mathcal{V}\}), \text{ where} \quad (1)$$

$$\mathcal{P}_{\mathcal{M}}(\mathcal{G}, v) = f_2(\mathbf{z}_{v, \mathcal{G}}, \ell_v)$$

The performance metric $\mathcal{P}_{\mathcal{M}}(\mathcal{G}, v)$ on node v is a function f_2 of its embedding $\mathbf{z}_{v, \mathcal{G}}$ and its ground truth label or score ℓ_v . The overall performance $\mathcal{P}_{\mathcal{M}}^*(\mathcal{G})$ is some aggregation f_1 over the performance across all nodes. We will discuss some specific instances in Section 4.

An adversarial attacker wishes to change \mathcal{G} by performing \mathcal{B} edge deletions and additions so that the performance on a *target node* t is minimized. We assume that the attacker has access to a subset of nodes $\mathcal{C} \subseteq \mathcal{V}$ and edges may be modified only among the set $\mathcal{C} \cup \{t\}$. Semantically, \mathcal{C} may represent colluding bots, or vulnerable users who have public profiles instead of private profiles, etc. Note that we do not explicitly allow node deletions and additions, since these can be modeled through deletions and additions over the edges (Dai et al. 2018).

Problem 1 (Targeted Black-box Evasion Attack)

Given graph $\mathcal{G} = (\mathcal{V}, \mathcal{E}, \mathcal{X})$, a target node t , budget \mathcal{B} , and a subset of accessible nodes $\mathcal{C} \subseteq \mathcal{V}$, perform at most \mathcal{B} edge additions or deletions from edge space $\{(u, v) \mid u, v \in \mathcal{C} \cup \{t\}\}$ to form graph \mathcal{G}^* such that

$$\mathcal{G}^* = \arg \min_{\mathcal{G}': d(\mathcal{G}, \mathcal{G}') \leq \mathcal{B}} \mathcal{P}_{\mathcal{M}}(\mathcal{G}', t) \quad (2)$$

Both the GNN model \mathcal{M} and performance metric $\mathcal{P}_{\mathcal{M}}(\mathcal{G}', t)$ are *unknown* to the attacker. Note that our formulation is easily extensible to a set of target nodes, where Eq. 2 is aggregated over all targets.

3 TANDIS: Targeted Attack via Neighborhood DISTortion

Since in the search process for \mathcal{G}^* , the attacker does not have access to either the performance metric $\mathcal{P}_{\mathcal{M}}^*(\mathcal{G})$ or the model-type of \mathcal{M} , we need a *surrogate* function $\phi(\mathcal{G}, t)$ in the *graph space*, such that if $distance(\phi(\mathcal{G}, t), \phi(\mathcal{G}', t)) \gg 0$ then $\mathcal{P}_{\mathcal{M}}(\mathcal{G}, t)$ is significantly different from $\mathcal{P}_{\mathcal{M}}(\mathcal{G}', t)$.

3.1 Neighbourhood Distortion in Graph Space

To identify $\phi(\mathcal{G}, t)$, we first note that there are primarily two types of GNNs:

- Neighborhood-convolution:** Examples of neighborhood convolution based architectures include GCN (Kipf and Welling 2017), GraphSage (Hamilton, Ying, and Leskovec 2017), and GAT (Velickovic et al. 2018). Here, the embedding of a node v is computed through a *convolution* operation ψ over its k -hop neighborhood, i.e., $\mathbf{z}_{v, \mathcal{G}} = \psi(\mathcal{N}_{\mathcal{G}}^k(v))$. Consequently, nodes with similar neighborhoods have similar embeddings (Xu et al. 2019b; You, Ying, and Leskovec 2019).

- Locality-aware:** In locality-aware GNNs such as P-GNN (You, Ying, and Leskovec 2019), GRAPHREACH (Nishad et al. 2021), DEEPWALK (Perozzi, Al-Rfou, and Skiena 2014), etc., two nodes have similar embeddings if

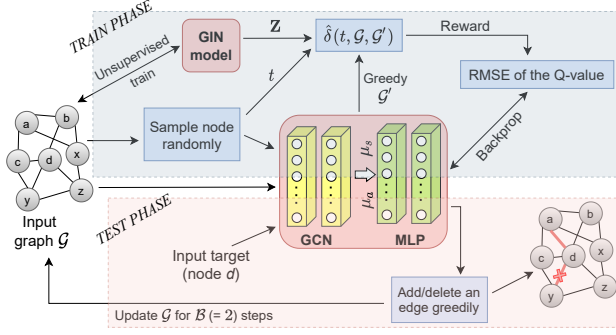


Figure 1: Pipeline of TANDIS in train and test phase.

they are located close to each other in the graph. Many real-world graphs display *small-world* and *scale-free* properties (Albert and Barabási 2002). Both small-world and scale-free graphs usually have high clustering coefficients, which indicate that one-hop neighbors share many other neighbors as well. Thus, nearby nodes have a high likelihood of having similar neighborhoods.

The above discussion reveals that node embeddings reflect node neighborhoods in both architectural paradigms. Consequently, the surrogate function $\phi(\mathcal{G}, t)$ may be set to target node t 's k -hop neighborhood $\mathcal{N}_{\mathcal{G}}^k(t)$. If $\mathcal{N}_{\mathcal{G}}^k(t)$ can be distorted through adversarial edge edits, then it would also perturb the embedding of t , which in turn would affect the performance metric. Towards that end, we define the notion of *neighborhood distortion* as follows.

Definition 1 (Neighborhood Distortion) Let $\mathcal{N}_{\mathcal{G}}^k(v)$ and $\mathcal{N}_{\mathcal{G}'}^k(v)$ be the k -hop neighborhoods of v in original graph \mathcal{G} and adversarially perturbed graph \mathcal{G}' respectively. The distortion in \mathcal{G}' with respect to a node v is simply the Jaccard distance of their neighborhoods.

$$\delta(v, \mathcal{G}, \mathcal{G}') = 1 - \frac{|\mathcal{N}_{\mathcal{G}}^k(v) \cap \mathcal{N}_{\mathcal{G}'}^k(v)|}{|\mathcal{N}_{\mathcal{G}}^k(v) \cup \mathcal{N}_{\mathcal{G}'}^k(v)|} \quad (3)$$

Problem 1 may now be reduced to the following objective:

$$\mathcal{G}^* = \arg \max_{\mathcal{G}': d(\mathcal{G}, \mathcal{G}') \leq \mathcal{B}} \delta(t, \mathcal{G}, \mathcal{G}') \quad (4)$$

where t is the target node. Unfortunately, maximizing $\delta(t, \mathcal{G}, \mathcal{G}')$ is NP-hard even for $k = 2$.

Theorem 1 The problem $\max_{\mathcal{G}': d(\mathcal{G}, \mathcal{G}') \leq \mathcal{B}} \delta(t, \mathcal{G}, \mathcal{G}')$ is NP-hard and the objective is non-monotone and non-submodular.

PROOF. We reduce the SET COVER problem to our maximization objective. See Appendix B in the full version for more details (Sharma et al. 2021).

Owing to NP-hardness, computing the optimal solution for the problem in Eq. 4 is not feasible. Furthermore, since the objective is neither submodular nor monotone, even the greedy algorithms that provide $1 - 1/e$ approximations are not applicable here (Nemhauser and Wolsey 1978). We, therefore, investigate other optimization strategies.

3.2 A Reinforcement Learning Approach for Neighborhood Distortion

Fig. 1 presents the pipeline of our proposed algorithm TANDIS. It proceeds through three phases.

- 1. Training data generation:** We capture a feature-space representation of node neighborhoods using *Graph Isomorphism Network* (GIN) (Xu et al. 2019b). This design choice is motivated by the property that GIN is as powerful as the *Weisfeiler-Lehman graph isomorphism test* (Xu et al. 2019b). On the feature space generated by GIN, we define a neighborhood distortion measure.
- 2. Train phase:** We train a deep Q -learning network (DQN), to predict the impact of an edge edit on distortion in the neighborhood embedding space. The proposed DQN framework captures the *combinatorial* nature of the problem, and shares *parameters across budgets*.
- 3. Test phase:** Given an unseen graph, we perform \mathcal{B} forward passes through the trained DQN in an iterative manner to form the answer set of \mathcal{B} edge edits.

3.3 Training Data Generation

The input to the training phase is a set of tuples of the form $\langle t, e, \mathcal{M}(\mathcal{G}), \mathcal{M}(\mathcal{G}_e) \rangle$. Here, t is the target node, e denotes an edge perturbation, and $\mathcal{M}(\mathcal{G}), \mathcal{M}(\mathcal{G}_e)$ are the GIN embeddings of the original graph \mathcal{G} and the graph formed following edge edit e, \mathcal{G}_e , respectively. $\mathcal{M}(\mathcal{G}) = \{\mathbf{Z}_v^{\mathcal{G}} \mid v \in \mathcal{V}\}$ contains the GIN embedding of each node in \mathcal{G} . $\mathbf{Z}_v^{\mathcal{G}}$ characterizes the k -hop neighborhood of node v in graph \mathcal{G} . t is randomly selected. The edge perturbations are selected using a greedy mechanism, which we detail in Appendix E of the full version (Sharma et al. 2021).

Embeddings via GIN: GIN draws its expressive power by deploying an *injective* aggregation function. Specifically, in the initial layer, each node is characterized by an *one-hot* vector of dimension $|\mathcal{V}|$, which encodes the node ID. Subsequently, in each hidden layer i , we learn an embedding through the following transformation.

$$\mathbf{h}_{v,i}^{\mathcal{G}} = MLP \left((1 + \epsilon^i) \cdot \mathbf{h}_{v,i-1}^{\mathcal{G}} + \sum_{u \in \mathcal{N}_{\mathcal{G}}^1(v)} \mathbf{h}_{u,i-1}^{\mathcal{G}} \right) \quad (5)$$

Here, ϵ^i is a layer-specific learnable parameter. The final embedding $\mathbf{Z}_v^{\mathcal{G}} = \mathbf{h}_{v,k}^{\mathcal{G}}$, where k is final hidden layer. The embeddings are learned by minimizing the following *unsupervised* loss function.

$$\mathcal{L}(\mathcal{M}(\mathcal{G})) = -\log(P(\mathcal{N}_{\mathcal{G}}^k(v) \mid \mathbf{Z}_v^{\mathcal{G}})), \text{ where} \quad (6)$$

$$P(\mathcal{N}_{\mathcal{G}}^k(v) \mid \mathbf{Z}_v^{\mathcal{G}}) = \prod_{u \in \mathcal{N}_{\mathcal{G}}^k(v)} P(u \mid \mathbf{Z}_v^{\mathcal{G}}) \text{ and} \quad (7)$$

$$P(u \mid \mathbf{Z}_v^{\mathcal{G}}) = \frac{\exp(\mathbf{Z}_u^{\mathcal{G}} \cdot \mathbf{Z}_v^{\mathcal{G}})}{\sum_{u' \in \mathcal{V}} \exp(\mathbf{Z}_{u'}^{\mathcal{G}} \cdot \mathbf{Z}_v^{\mathcal{G}})} \quad (8)$$

For the pseudocode, please refer to Appendix C of Sharma et al. (2021).

Distortion in embedding space: We define distortion in the perturbed graph \mathcal{G}' with respect to the original graph \mathcal{G} as follows:

$$\widehat{\delta}(t, \mathcal{G}, \mathcal{G}') = d_o(t) - d_p(t) \quad (9)$$

Here, $d_o(t) = \frac{1}{|\mathcal{N}_{\mathcal{G}}^k(t)|} \sum_{u \in \mathcal{N}_{\mathcal{G}}^k(t)} \left\| \mathbf{z}_t^{\mathcal{G}'} - \mathbf{z}_u^{\mathcal{G}'} \right\|_2$ denotes the *mean L2 distance* in the *perturbed embedding* space between target node t and the nodes in its original unperturbed neighborhood. On the other hand, $d_p(t) = \frac{1}{|\mathcal{N}_{\mathcal{G}'}^k(t)|} \sum_{u \in \mathcal{N}_{\mathcal{G}'}^k(t)} \left\| \mathbf{z}_t^{\mathcal{G}'} - \mathbf{z}_u^{\mathcal{G}'} \right\|_2$ denotes the same between target node t and the nodes in its *perturbed* neighborhood.

In our formulation, if the neighborhood remains unchanged, then $d_o(t) = d_p(t)$, and hence distortion is 0. The distortion will be maximized if the distance of the target node to the original neighbors become significantly higher in the perturbed space than the distance to the neighbors in the perturbed graph. With the above definition of distortion in the embedded space, the maximization objective in Eq. 4 is approximated as :

$$\mathcal{G}^* = \arg \max_{\mathcal{G}' : d(\mathcal{G}, \mathcal{G}') \leq \mathcal{B}} \widehat{\delta}(t, \mathcal{G}, \mathcal{G}') \quad (10)$$

This approximation is required due to two reasons: **(1)** Maximizing Eq. 4 is NP-hard, and **(2)** Eq. 4 is not differentiable.

3.4 Learning Q-function

We optimize Eq. 10 via Q-learning (Sutton and Barto 2018), which inherently captures the combinatorial aspect of the problem in a budget-independent manner. As depicted in Fig. 2, our deep Q-learning framework is an *end-to-end* architecture with a sequence of two separate neural components, a graph neural network (in experiments, we use GCN (Kipf and Welling 2017)) and a separate Multi-layer Perceptron (MLP) with the corresponding learned parameter set Θ_Q . Given a set of edges S and an edge $e \notin S$, we predict the n -step reward, $Q_n(S, e)$, for including e to the solution set S via the surrogate function $Q'_n(S, e; \Theta_Q)$.

Defining the framework: The Q-learning task is defined in terms of state space, action space, reward, policy, and termination condition.

- **State space:** The state space characterizes the state of the system at any time step i . Since our goal is to distort the neighborhood of target node t , we define it in terms of its k -hop neighborhood $\mathcal{N}_{\mathcal{G}_i}^k(t)$. Note that the original graph evolves at each step through edge edits. \mathcal{G}_i denotes the graph at time step i . The representation of state s_i is defined as:

$$\boldsymbol{\mu}_{s_i} = \sum_{v \in \mathcal{N}_{\mathcal{G}_i}^k(t)} \boldsymbol{\mu}_v \quad (11)$$

where $\boldsymbol{\mu}_v$ is the embedding of node v learned using a GNN (GCN in our implementation).

- **Action:** An action, a_i at i -th step corresponds to adding or deleting an edge $e = (v, t)$ to the solution set S_{i-1} where the target node is t . The representation of the action a_i is:

$$\boldsymbol{\mu}_{a_i} = \pm \text{CONCAT}(\boldsymbol{\mu}_v, \boldsymbol{\mu}_t), \quad (12)$$

where the sign denotes edge addition (+) and deletion (-) actions.

- **Reward:** The immediate (0-step) reward of action a_i is its *marginal gain* in distortion, i.e.,

$$r(s_i, a_i) = \widehat{\delta}(t, \mathcal{G}_i, \mathcal{G}_{i+1}) \quad (13)$$

where \mathcal{G}_{i+1} is the graph formed due to a_i on \mathcal{G}_i .

- **Policy and Termination:** At the i -th step, the policy $\pi(e | S_{i-1})$ selects the edge with the highest *predicted* n -step reward, i.e., $\arg \max_{e \in C_t} Q'_n(S_i, e; \Theta_Q)$, where

$$Q'_n(S_i, e = (u, t); \Theta_Q) = \mathbf{w}_1^T \cdot \sigma(\boldsymbol{\mu}_{s_i, a_i}), \text{ where} \quad (14)$$

$$\boldsymbol{\mu}_{s_i, a_i} = \mathbf{W}_2 \cdot \text{CONCAT}(\boldsymbol{\mu}_{s_i}, \boldsymbol{\mu}_{a_i})$$

$\mathbf{w}_1, \mathbf{W}_2$ are learnable weight vector and matrix respectively. We terminate training after T samples.

Learning the Parameter Set Θ_Q : Θ_Q consists of weight vector \mathbf{w}_1 , and weight matrices \mathbf{W}_2 , and $\{\mathbf{W}_{GCN}^l\}$. While \mathbf{w}_1 and \mathbf{W}_2 are used to compute $Q'_n(S_i, e)$, \mathbf{W}_{GCN}^l are parameters of the GCN for each hidden layer $l \in [1, k]$. Q-learning updates parameters in a single episode via *Adam optimizer* (Kingma and Ba 2014) minimizing the *squared loss*.

$$J(\Theta_Q) = (y - Q'_n(S_i, e_i; \Theta_Q))^2, \text{ where}$$

$$y = \gamma \cdot \max_{e=(u,t), u \in C} \{Q'_n(S_{i+n}, e; \Theta_Q)\} + \sum_{j=0}^{n-1} r(S_{i+j}, e_{i+j})$$

The *discount factor* γ balances the importance of immediate reward with the predicted n -step future reward (Sutton and Barto 2018). The pseudocode with additional details is provided in the full version (Sharma et al. 2021).

3.5 Test phase

Given an unseen graph \mathcal{G} with budget \mathcal{B} , we perform \mathcal{B} forward passes through the DQN. Each forward pass returns the edge with the highest predicted long-term reward and updates the state space representations. Note that the GIN is not used in the test phase. It is only used for training the DQN. Furthermore, the proposed inference pipeline is also independent of the test GNN or the loss function since it directly attacks the target node neighborhood.

3.6 Complexity Analysis

Here, we analyze the running time complexity of TANDIS during test phase. The complexity analysis for the train phase is provided in Appendix F in the full version (Sharma et al. 2021) along with a complete proof of the obtained test-time complexity.

Test phase involves finding $Q'_n(S_i, e)$ by doing a forward pass on a k -layer GCN followed by an L -layer MLP. We ignore the effects of the number of layers k, L . Combining the costs from both GCN and MLP, and the fact that we make \mathcal{B} forward passes, the total computation complexity is $O(\mathcal{B}(|\mathcal{E}|h_g + |\mathcal{V}|h_g^2 + |\mathcal{V}|(h_m(1 + h_g))))$. Since h_g and h_m may be considered as constants, the complexity with respect to the input parameters reduces to $O(\mathcal{B}(|\mathcal{E}| + |\mathcal{V}|))$.

4 Empirical Evaluation

We evaluate TANDIS across *three downstream tasks* of link prediction (**LP**), node classification (**NC**) and pairwise node classification (**PNC**) (You, Ying, and Leskovec 2019; Nishad et al. 2021). We provide additional details about

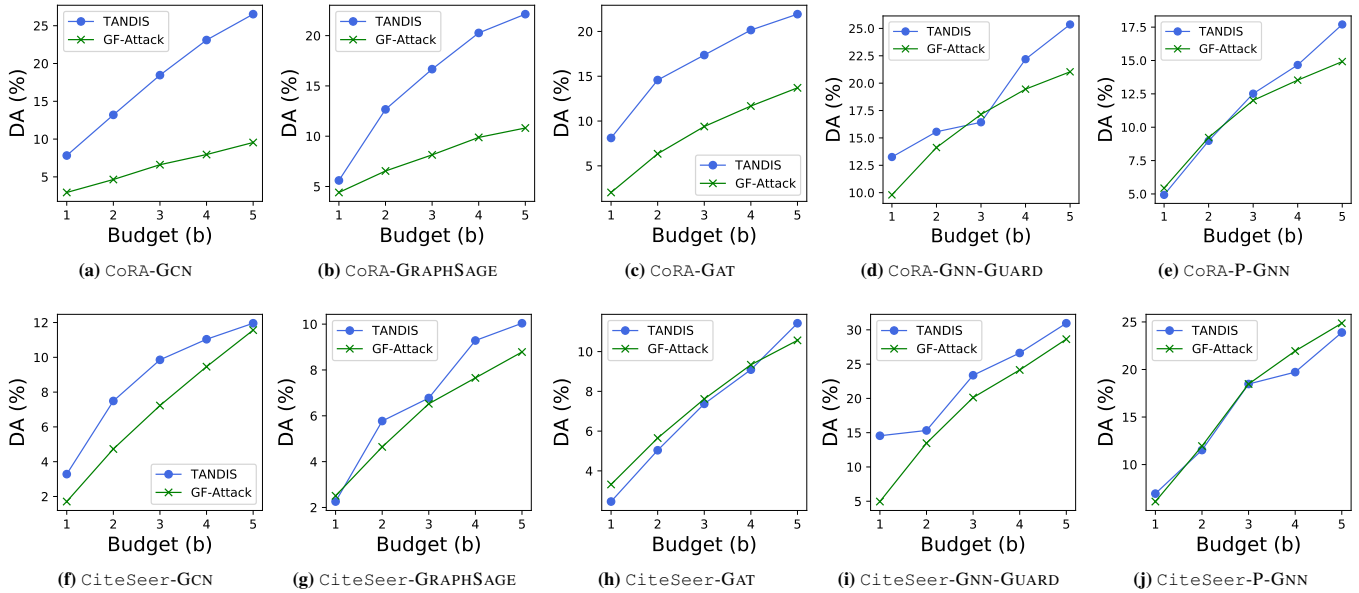


Figure 2: Link prediction: Percentage drop in accuracy (DA) in different models with varying budget in (a-d) CoRA and (e-h) CiteSeer. Higher means better.

Budget	Dataset	CoRA					CiteSeer				
		GCN	SAGE	GAT	Guard	P-GNN	GCN	SAGE	GAT	Guard	P-GNN
(unatk)		81.6	80.8	83.9	83.4	78.3	73.9	76.1	74.9	75.2	74.6
$\mathcal{B} = 1$	RL-S2V	3.4	3.8	3.8	7.4	7.9	4.6	5.7	4.0	9.9	3.3
	GF-ATTACK	5.0	2.9	1.7	2.5	3.3	4.9	4.9	20.8	4.3	3.7
	TANDIS	19.2	2.6	8.0	12.6	4.9	33.2	10.8	6.9	7.5	4.1
$\mathcal{B} = 5$	RL-S2V	7.6	7.9	8.8	15.3	16.6	10.2	13.8	11.1	28.6	8.0
	GF-ATTACK	22.6	16.8	21.5	20.6	15.1	35.5	22.0	34.7	18.0	14.8
	TANDIS	42.5	14.5	21.5	26.7	29.5	44.9	23.1	26.4	13.6	10.7
$\mathcal{B} = 10$	GF-ATTACK	36.3	25.2	34.6	30.0	25.0	52.8	30.0	44.8	28.4	24.9
	TANDIS	47.2	23.0	35.2	31.9	60.0	54.4	31.1	44.9	22.7	19.6
$\mathcal{B} = 20$	GF-ATTACK	53.6	38.0	48.3	42	45.8	67.5	38.1	61.4	39.2	37.8
	TANDIS	58.1	40.5	53.4	42	81.1	61.2	40.6	65.4	37.1	38.7

Table 2: Node Classification: Drop in DA against budget. We denote GRAPH SAGE and GNN-GUARD as SAGE and Guard respectively. “unatk” represents the accuracy before attack.

the experimental setup in Appendix G of the full version (Sharma et al. 2021). Our code base is shared in the supplementary package.

Datasets: We use three standard real-world datasets in our experiments following (Chang et al. 2020): CoRA (McCallum et al. 2000), CiteSeer and PubMed (Sen et al. 2008). For more details, refer Appendix G of the full version (Sharma et al. 2021).

Baselines: We compare with GF-ATTACK (Chang et al. 2020), which is the closest in terms of features except being model-agnostic (for which, we can exploit transferability of attacks) (Recall Table 1). We also compare with RL-S2V (Dai et al. 2018), which is model-agnostic but not task-agnostic (limited to node classification). We also include non-neural baselines in the full version (Sharma et al. 2021) such as (i) *random perturbations*, (ii) *degree centrality*, and (iii) *greedy*.

In this context, Bojchevski and Günnemann (2019) also

attacks GNNs through an idea based on neighborhood distortion. However, we do not compare against it since it is a poisoning attack. Poisoning attacks perturb the training data instead of test data as in our case. Furthermore, when this algorithm is adapted for evasion attacks, our main baseline GF-ATTACK (Chang et al. 2020) outperforms significantly.

Target models: We test the efficacy of our attacks on five state-of-the-art GNN models in our experiments: (1) GCN (Kipf and Welling 2017), (2) GRAPH SAGE (Hamilton, Ying, and Leskovec 2017), (3) GAT (Velickovic et al. 2018), (4) P-GNN (You, Ying, and Leskovec 2019), and (5) GNN-GUARD (Zhang and Zitnik 2020). The first three are based on *neighborhood-convolution*, P-GNN is locality-aware, and GNN-GUARD is a GNN model specifically developed to avert adversarial poisoning attacks.

Parameters: We use a 2-layer GIN in TANDIS to quantify distortion while training. To train the attack models, we use 10% nodes each for training and validation and 80% for test.

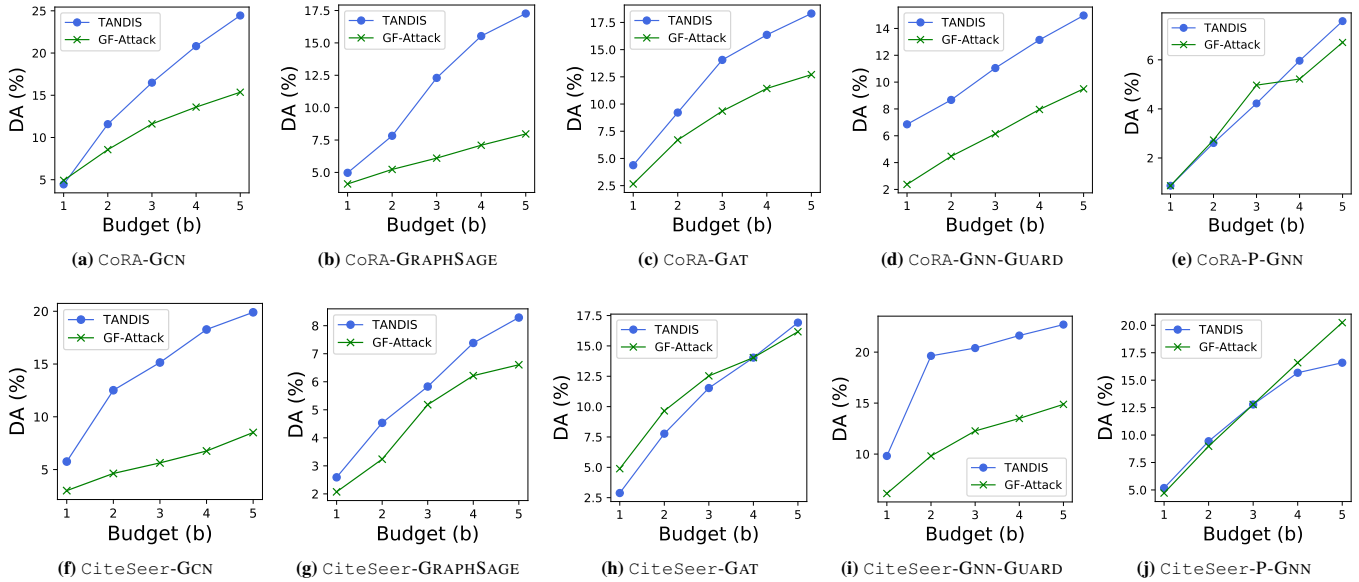


Figure 3: **Pairwise node classification: Percentage drop in accuracy (DA) in (a-d) CoRA and (e-h) CiteSeer. Higher means better.**

On the test set, we ensure that the class distribution is balanced by down-sampling the majority class. Other details regarding the hyperparameters are mentioned in Sharma et al. (2021).

Metric: We quantify the attack performance using the percentage change in accuracy before and after attack, i.e. *Drop-in-Accuracy (DA%)*, defined as

$$DA(\%) = \frac{\text{Original Accuracy} - \text{Accuracy after attack}}{\text{Original Accuracy}} \times 100. \quad (15)$$

4.1 Impact of Perturbations

In this section, we compare TANDIS with relevant baselines on CiteSeer and CoRA. Since both GF-ATTACK and RL-S2V fail to scale for higher budgets on PubMed, we defer the results on PubMed to Section 4.2.

Link Prediction (LP): Fig. 2 evaluates the performance on LP. TANDIS consistently produces better results i.e., higher drop in accuracy, in most cases. The only exception are GAT and P-GNN in CiteSeer (Figures 2h, 2j). In these cases, the drop in accuracy is similar for TANDIS and GF-ATTACK. Another interesting observation that emerges from this experiment is that the drop in accuracy in GNN-GUARD is higher than the standard GNN models. This is unexpected since GNN-GUARD is specifically designed to avert adversarial attacks. However, it must be noted that GNN-GUARD was designed to avert poisoning attacks, whereas TANDIS launches an evasion attack. This indicates that defence mechanisms for poisoning attacks might not transfer to evasion attacks.

Pairwise Node Classification (PNC): Here, the task is to predict if two nodes belong to the same class or not. Figure 3 shows that TANDIS is better across all models except in GAT on CiteSeer, where both obtain similar performance.

Node Classification (NC): Table 2 presents the results on NC. Since RL-S2V is prohibitively slow in inference, we

report results till $\mathcal{B} = 5$ for RL-S2V. TANDIS outperforms GF-ATTACK and RL-S2V in majority of the cases. However, the results in NC are more competitive. Specifically, GF-ATTACK outperforms TANDIS in a larger number of cases than in LP and PNC. A deeper analysis reveals that attacking NC is an easier task than LP and PNC. This is evident from the observed drop in accuracy in NC, which is significantly higher than in LP and PNC. Consequently, it is harder for one technique to significantly outshine the other.

Summary: Overall, three key observations emerge from these experiments. First, it is indeed possible to launch task and model agnostic attacks on GNN models. Second, TANDIS, on average, produces a drop in accuracy that is more than 50% (i.e., 1.5 times) higher than GF-ATTACK. Third, neighborhood distortion is an effective mechanism to perturb graphs and, hence, potential solutions to defence strategies may lie in recognizing and deactivating graph links that significantly distort node neighborhoods.

4.2 Impact on PubMed

Efficacy: Consistent with previous results, the impact of TANDIS on NC is higher than in LP and PNC (See Figs. 4a-4c). Furthermore, we note that P-GNN and GRAPH-SAGE are more robust than other models. We are unable to include GF-ATTACK in these plots due to its high inference times. Nonetheless, we compare with GF-ATTACK and RL-S2V for budget = 1 in Table 3. As visible, TANDIS obtains the best performance in most of the cases.

4.3 Running Time

Figure 4d compares the inference times of TANDIS and the second-best baseline GF-ATTACK, i.e. the running time of finding black-box perturbations. We do not compare with RL-S2V, since it fails to complete running for any $\mathcal{B} > 1$ even after 10 hours. TANDIS (represented by solid lines) is more than 3 orders of magnitude faster than GF-ATTACK for

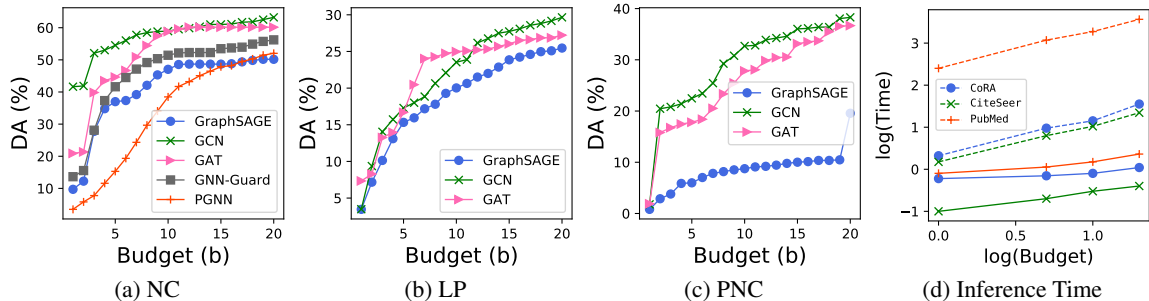


Figure 4: Performance of TANDIS in the PubMed dataset (a-c), (d) Inference times of TANDIS (solid lines) and GF-ATTACK (dashed lines) against budget.

Models	Link Prediction			Pairwise NC		
	GCN	SAGE	GAT	GCN	SAGE	GAT
GF-ATTACK	5.6	4.4	6.4	0.2	0.6	0.4
TANDIS	3.5	3.4	7.4	0.8	1.8	1.2

(a) LP and PNC

Models	GCN	SAGE	GAT	P-GNN	GNN-GUARD
(unattacked)	86.2	86.5	87.6	86.3	83.6
RL-S2V	2.8	2.3	2.7	2.1	5.2
GF-ATTACK	36.9	3.8	36.5	3.4	11.7
TANDIS	41.6	9.7	20.9	3.5	13.7

(b) NC

Table 3: Drop in accuracy (DA) in PubMed at budget = 1.

the largest dataset, PubMed. Also, time taken by TANDIS grows at a much lower rate with the increase in budget than GF-ATTACK. Furthermore, TANDIS requires training only once per dataset and the entire training procedure takes upto 3 hours even for the largest dataset, i.e. PubMed.

4.4 Potential Detection Mechanisms

Here, we conduct an experiment on CoRA dataset to find correlations between perturbations chosen by our attacks and the ones chosen according to common network properties. The aim is to (1) interpret our attacks in graph space and (2) identify potential ways to catch our evading attack.

In particular, we consider all node pairs of the form (t, v) , where t is the target and v is the node to which an edge may be added or removed. We characterize each v with several graph level properties such as clustering coefficient, conductance, etc (See Sharma et al. (2021) for the complete list). Corresponding to each property, we create a sorted list P of nodes in descending order of their property values. Similarly, we create another list D with nodes that are sorted

Feature	Correlation (p-value)
Feature Similarity (fs)	$-0.20^* \pm 0.196$
Degree (dg)	$-0.15^* \pm 0.008$
Local Clustering Coeff. (cc)	$+0.25^* \pm 0.004$

Table 4: Correlation of node properties with neighborhood distortion (* indicates $p < 0.001$).

based on the distortion produced due to removal/addition of edge (t, v) . We next compute the Spearman’s rank correlation coefficient between P and D and its p -value. Properties with statistically significant correlations may indicate graph-level features that govern the selection of perturbations by TANDIS and thus, effective in detecting these attacks.

Table 4 presents the properties that are statistically significant. These results indicate that edges to nodes of high clustering coefficient (cc) lead to large distortion. This result is not surprising since a node with high cc short-circuits the target node to a large number of nodes (or removes this short-circuit in case of edge deletion). The negative correlation with fs is also intuitive, since low fs with a node indicates that an edge to it injects a large amount of heterophily. The results for dg is rather surprising, where a negative correlation indicates that edges to low-degree nodes are more effective. A deeper analysis reveals that dg is negatively correlated with cc , which may explain the negative correlation with distortion as well. Note that, in GF-ATTACK, it has been shown that perturbing edges with high degree nodes is not an effective attack strategy. Our study is consistent with that result, while also indicating that cc is a more effective graph-level parameter.

5 Conclusions

GNNs have witnessed widespread usage for several tasks such as node classification and link prediction. Hence, assessing its robustness to practical adversarial attacks is important to test their applicability in security-critical domains. While the literature on adversarial attacks for GNNs is rich, they are built under the assumption that the attacker has knowledge of the specific GNN model used to train and/or the prediction task being attacked. The key insight in our proposed work is that simply distorting the neighborhood of the target node leads to an effective attack regardless of the underlying GNN model or the prediction task. Hence, hiding the model or the task information from the attacker is not enough. We also find that such perturbations are not correlated with simple network properties and may be hard to detect. Our work thus opens new avenues of research that can focus on defending and detecting such practical attacks to analyze why such perturbations should transfer across different tasks and victim models.

Acknowledgements

We thank the HPC facility of IIT Delhi for computational resources and the reviewers for their constructive feedback.

References

- Albert, R.; and Barabási, A.-L. 2002. Statistical mechanics of complex networks. *Reviews of modern physics*, 74(1): 47.
- Bhattoo, R.; Ranu, S.; and Krishnan, N. M. A. 2022. Learning Articulated Rigid Body Dynamics with Lagrangian Graph Neural Network. In *Advances in Neural Information Processing Systems*.
- Bojchevski, A.; and Günnemann, S. 2019. Adversarial Attacks on Node Embeddings via Graph Poisoning. In *Proceedings of the 36th International Conference on Machine Learning, ICML*.
- Chang, H.; Rong, Y.; Xu, T.; Huang, W.; Zhang, H.; Cui, P.; Zhu, W.; and Huang, J. 2020. A Restricted Black-Box Adversarial Framework Towards Attacking Graph Embedding Models. In *Proceedings of the AAAI Conference on Artificial Intelligence*.
- Chen, J.; Zhang, D.; Ming, Z.; and Huang, K. 2021. GraphAttacker: A General Multi-Task GraphAttack Framework. *arXiv preprint arXiv:2101.06855*.
- Dai, H.; Li, H.; Tian, T.; Huang, X.; Wang, L.; Zhu, J.; and Song, L. 2018. Adversarial attack on graph structured data. In *Proceedings of the 35th International Conference on Machine Learning, ICML*, 1115–1124.
- Goyal, N.; Jain, H. V.; and Ranu, S. 2020. GraphGen: A Scalable Approach to Domain-agnostic Labeled Graph Generation. In *Proceedings of The Web Conference 2020*, 1253–1263.
- Grover, A.; and Leskovec, J. 2016. node2vec: Scalable feature learning for networks. In *Proceedings of the 22nd ACM SIGKDD International Conference on Knowledge Discovery and Data Mining*, 855–864.
- Gupta, V.; and Chakraborty, T. 2021. Adversarial Attack on Network Embeddings via Supervised Network Poisoning. *arXiv preprint arXiv:2102.07164*.
- Hamilton, W. L.; Ying, Z.; and Leskovec, J. 2017. Inductive representation learning on large graphs. In *Advances in Neural Information Processing Systems*, 1024–1034.
- Jain, A.; Liu, I.; Sarda, A.; and Molino, P. 2019. Food Discover with Uber Eats.
- Jain, J.; Bagadia, V.; Manchanda, S.; and Ranu, S. 2021. NeuroMLR: Robust & Reliable Route Recommendation on Road Networks. *Advances in Neural Information Processing Systems*, 34: 22070–22082.
- Kingma, D. P.; and Ba, J. 2014. Adam: A Method for Stochastic Optimization.
- Kipf, T. N.; and Welling, M. 2017. Semi-Supervised Classification with Graph Convolutional Networks. In *International Conference on Learning Representations (ICLR)*.
- Li, J.; Zhang, H.; Han, Z.; Rong, Y.; Cheng, H.; and Huang, J. 2020. Adversarial attack on community detection by hiding individuals. In *Proceedings of the Web Conference 2020*.
- Liu, X.; Si, S.; Zhu, J.; Li, Y.; and Hsieh, C.-J. 2019. A Unified Framework for Data Poisoning Attack to Graph-based Semi-supervised Learning. In *Advances in Neural Information Processing Systems*.
- Ma, J.; Ding, S.; and Mei, Q. 2020. Towards More Practical Adversarial Attacks on Graph Neural Networks. *Advances in neural information processing systems*.
- Ma, Y.; Wang, S.; Derr, T.; Wu, L.; and Tang, J. 2019. Attacking graph convolutional networks via rewiring. *arXiv preprint arXiv:1906.03750*.
- Manchanda, S.; Mittal, A.; Dhawan, A.; Medya, S.; Ranu, S.; and Singh, A. 2020. GCOMB: Learning Budget-constrained Combinatorial Algorithms over Billion-sized Graphs. *Advances in Neural Information Processing Systems*, 33.
- McCallum, A. K.; Nigam, K.; Rennie, J.; and Seymore, K. 2000. Automating the construction of internet portals with machine learning. *Information Retrieval*, 3(2): 127–163.
- Nemhauser, G. L.; and Wolsey, L. A. 1978. Best algorithms for approximating the maximum of a submodular set function. *Mathematics of operations research*, 3(3): 177–188.
- Nishad, S.; Agarwal, S.; Bhattacharya, A.; and Ranu, S. 2021. GraphReach: Locality-Aware Graph Neural Networks using Reachability Estimations. In *Proceedings of the 30th International Joint Conference on Artificial Intelligence*.
- Pal, A.; Eksombatchai, C.; Zhou, Y.; Zhao, B.; Rosenberg, C.; and Leskovec, J. 2020. PinnerSage: Multi-Modal User Embedding Framework for Recommendations at Pinterest. In *Proceedings of the 26th ACM SIGKDD International Conference on Knowledge Discovery and Data Mining*.
- Perozzi, B.; Al-Rfou, R.; and Skiena, S. 2014. DeepWalk: Online learning of social representations. In *Proceedings of the 20th ACM SIGKDD International Conference on Knowledge Discovery and Data Mining*, 701–710.
- Ranjan, R.; Grover, S.; Medya, S.; Chakaravarthy, V.; Sabharwal, Y.; and Ranu, S. 2022. GREED: A Neural Framework for Learning Graph Distance Functions. In *Advances in Neural Information Processing Systems*.
- Sen, P.; Namata, G.; Bilgic, M.; Getoor, L.; Galligher, B.; and Eliassi-Rad, T. 2008. Collective classification in network data. *AI magazine*, 29(3): 93–93.
- Sharma, K.; Verma, S.; Medya, S.; Ranu, S.; and Bhattacharya, A. 2021. Task and Model Agnostic Adversarial Attack on Graph Neural Networks. *arXiv preprint arXiv:2112.13267*.
- Sun, L.; Wang, J.; Yu, P. S.; and Li, B. 2018. Adversarial Attack and Defense on Graph Data: A Survey. *CoRR*, abs/1812.10528.
- Sun, Y.; Wang, S.; Tang, X.; Hsieh, T.-Y.; and Honavar, V. 2020. Adversarial Attacks on Graph Neural Networks via Node Injections: A Hierarchical Reinforcement Learning Approach. In *Proceedings of the Web Conference 2020*.
- Sutton, R. S.; and Barto, A. G. 2018. *Reinforcement learning: An introduction*. MIT press.

Thangamuthu, A.; Kumar, G.; Bishnoi, S.; Bhattoo, R.; Krishnan, N. M. A.; and Ranu, S. 2022. Unravelling the Performance of Physics-informed Graph Neural Networks for Dynamical Systems. In *Thirty-sixth Conference on Neural Information Processing Systems Datasets and Benchmarks Track*.

Velickovic, P.; Cucurull, G.; Casanova, A.; Romero, A.; Liò, P.; and Bengio, Y. 2018. Graph Attention Networks. In *International Conference on Learning Representations (ICLR)*.

Wang, B.; and Gong, N. Z. 2019. Attacking Graph-Based Classification via Manipulating the Graph Structure. In *SIGSAC, 2023–2040*.

Wang, B.; Zhou, T.; Lin, M.; Zhou, P.; Li, A.; Pang, M.; Fu, C.; Li, H.; and Chen, Y. 2020. Efficient Evasion Attacks to Graph Neural Networks via Influence Function. *arXiv preprint arXiv:2009.00203*.

Wu, H.; Wang, C.; Tyshetskiy, Y.; Docherty, A.; Lu, K.; and Zhu, L. 2019. Adversarial Examples for Graph Data: Deep Insights into Attack and Defense. In *Proceedings of the 28th International Joint Conference on Artificial Intelligence*.

Xu, K.; Chen, H.; Liu, S.; Chen, P.-Y.; Weng, T.-W.; Hong, M.; and Lin, X. 2019a. Topology Attack and Defense for Graph Neural Networks: An Optimization Perspective. In *Proceedings of the 28th International Joint Conference on Artificial Intelligence*.

Xu, K.; Hu, W.; Leskovec, J.; and Jegelka, S. 2019b. How Powerful are Graph Neural Networks? In *International Conference on Learning Representations (ICLR)*.

You, J.; Ying, R.; and Leskovec, J. 2019. Position-aware Graph Neural Networks. In *Proceedings of the 36th International Conference on Machine Learning, ICML, 7134–7143*.

Zhang, H.; Zheng, T.; Gao, J.; Miao, C.; Su, L.; Li, Y.; and Ren, K. 2019. Data Poisoning Attack against Knowledge Graph Embedding. In *Proceedings of the 28th International Joint Conference on Artificial Intelligence*.

Zhang, X.; and Zitnik, M. 2020. GNNGuard: Defending Graph Neural Networks against Adversarial Attacks. In *Advances in Neural Information Processing Systems*.

Zügner, D.; Akbarnejad, A.; and Günnemann, S. 2018. Adversarial attacks on neural networks for graph data. In *Proceedings of the 24th ACM SIGKDD International Conference on Knowledge Discovery and Data Mining, 2847–2856*.

Zügner, D.; and Günnemann, S. 2019. Adversarial Attacks on Graph Neural Networks via Meta Learning. In *International Conference on Learning Representations (ICLR)*.

Appendix

A Attack taxonomy

- **Poisoning attacks:** In poisoning attacks, the attacker injects adversarial samples in the training data, so that the accuracy of the predictive task being modeled is compromised (Bojchevski and Günnemann 2019; Gupta and Chakraborty 2021; Li et al. 2020; Liu et al. 2019; Sun et al. 2020; Wang and Gong 2019; Xu et al. 2019a; Zhang et al. 2019; Zügner, Akbarnejad, and Günnemann 2018; Zügner and Günnemann 2019). Note that (Bojchevski and Günnemann 2019) also addresses attacks on embedding, however we do not compare it against our method as it is a poisoning attack and one of our baselines, GF-ATTACK (Chang et al. 2020) clearly outperforms this on the ode classification task.
- **Evasion attacks:** In evasion attacks, the attacker adversarially modifies the test graph, so that the accuracy on the test graph is compromised (Chang et al. 2020; Chen et al. 2021; Dai et al. 2018; Ma, Ding, and Mei 2020; Ma et al. 2019; Wang et al. 2020; Wu et al. 2019; Xu et al. 2019a; Zügner, Akbarnejad, and Günnemann 2018). A modification may involve addition or deletion of nodes and edges, or changing node attributes. Note that the trained model remains unchanged.

Since an evasion attack relies only on the test data, it is comparatively easier to launch than a poisoning attack. As an example, consider the task of friend recommendation (link prediction) in a social network such as Facebook. It is easier for an attacker to infuse bots in Facebook that send friend requests (edge rewiring) to strategically selected users than getting access to Facebook’s training model.

B PROOF OF THM. 1

NP-hardness We reduce the SET COVER problem to our maximization objective for $k = 2$.

Definition 2 (Set Cover) *Given a collection of subsets $S = \{S_1, \dots, S_m\}$ from a universe of items $U = \{u_1, \dots, u_n\}$ and a budget b , determine if there exists a set of b subsets $\mathcal{A} \subseteq S$ such that $\cup_{S_i \in \mathcal{A}} S_i = U$, $|\mathcal{A}| = b$.*

Let $(U = \{u_1, \dots, u_n\}, S = \{S_1, \dots, S_m\}, b)$ be an instance of the SET COVER problem. We map this to an instance of our problem via constructing a graph $\mathcal{G} = (\mathcal{V}, \mathcal{E})$ as follows. From S and U , we create two sets of nodes $X = \{x_i \mid S_i \in S\}$ and $Y = \{y_j \mid u_j \in U\}$ respectively. We also add an additional node t with no edges attached to it. Thus, $\mathcal{V} = X \cup Y \cup \{t\}$. Additionally, if $u_j \in S_i$, an edge (x_i, y_j) is added to the edge set \mathcal{E} . The set of colluding nodes is set to $\mathcal{C} = X$, budget $\mathcal{B} = r$, and the target node is t . In this construction, if \mathcal{A} is a solution set of the SET COVER instance, then the corresponding set of edge additions $B = \{(t, x_i) \mid S_i \in \mathcal{A}\}$ maximizes $\delta(t, \mathcal{G}, \mathcal{G}')$. Specifically, $\mathcal{N}_{\mathcal{G}}^2(t) = \emptyset$ since no edges are incident on it. Thus, maximizing $\delta(t, \mathcal{G}, \mathcal{G}')$ is equivalent to maximizing $|\mathcal{N}_{\mathcal{G}}^2(t)|$. The maximum value of $|\mathcal{N}_{\mathcal{G}}^2(t)| = b + n$ if and only if \mathcal{A} is a set cover. \square

Non-montone We first define $\delta(v, \mathcal{G}, \mathcal{G}')$ as a set function:

$$\delta(v, \mathcal{G}, \mathcal{G}') := f(\mathcal{N}_{\mathcal{G}'}^k(v); \mathcal{N}_{\mathcal{G}}^k(v)) = 1 - \frac{|\mathcal{N}_{\mathcal{G}}^k(v) \cap \mathcal{N}_{\mathcal{G}'}^k(v)|}{|\mathcal{N}_{\mathcal{G}}^k(v) \cup \mathcal{N}_{\mathcal{G}'}^k(v)|}$$

Hence, the objective can be written as a set function as

$$f(A; B) = 1 - \frac{|A \cap B|}{|A \cup B|}$$

Consider a set S and $x \notin S$. Now, we have two cases:

Case (1) $x \in B$: $f(S \cup \{x\}; B) - f(S; B) = \frac{|S \cap B|}{|S \cup B|} - \frac{|(S \cup \{x\}) \cap B|}{|(S \cup \{x\}) \cup B|} = \frac{-1}{|S \cup B|} < 0$.

Case (2) $x \notin B$: $f(S \cup \{x\}; B) - f(S; B) = \frac{|S \cap B|}{|S \cup B|} - \frac{|(S \cup \{x\}) \cap B|}{|(S \cup \{x\}) \cup B|} = |S \cap B| \left(\frac{1}{|S \cup B|} - \frac{1}{|S \cup B| + 1} \right) > 0$.

Hence, f is not monotonic and the sign of its change depends on whether $x \in B$ or $x \notin B$. \square

Non-submodular

Definition 3 (Submodularity) *A set-function h is submodular if for every sets X, Y such that $X \subseteq Y$, and for every $e \notin Y$,*

$$h(X \cup \{e\}) - h(X) \geq h(Y \cup \{e\}) - h(Y).$$

Consider f as defined above. We consider two sets S, T such that $S \subset T$. Let $x \notin T$ but $x \in B$. Then, $f(S \cup \{x\}; B) - f(S; B) = \frac{-1}{|S \cup B|}$, and $f(T \cup \{x\}; B) - f(T; B) = \frac{-1}{|T \cup B|}$. Thus, $(f(S \cup \{x\}; B) - f(S; B)) - (f(T \cup \{x\}; B) - f(T; B)) = \frac{1}{|T \cup B|} - \frac{1}{|S \cup B|} < 0$.

Therefore, the objective f is not submodular. \square

C Expressive power of GIN

Pseudo-code of GIN In Section 3.3, GIN is trained in an unsupervised manner minimizing the loss given in Equation 6. In particular, we apply negative-sampling (Hamilton, Ying, and Leskovec 2017) to approximate the following loss function:

$$\mathcal{L}(\mathcal{M}(\mathcal{G})) = -\log(\sigma(\mathbf{Z}_u^T \mathbf{Z}_v)) - \mathbb{E}_{v_n \sim P_n(v)} \log(\sigma(-\mathbf{Z}_u^T \mathbf{Z}_{v_n})) \quad (16)$$

where $P_n(v)$ denotes a distribution of nodes which do not have an edge with v and v_n is negatively sampled from this distribution. σ denotes the activation function Sigmoid.

For training, we sample a set of positive and negative random walks and optimize the total loss in a batch for a fixed number of epochs. Therefore, v in Equation 16 denotes the nodes in a positive random walk, which is derived from a random walker. Similarly, v_n denotes the nodes in a negative random walk, i.e., v_n is a randomly chosen node in the whole graph. Algorithm 1 shows the entire process.

Expressive Power of GIN In this section, we explain the reasons of why a GIN model would be the most effective choice in the case of a black-box model. Since our attack must be model-agnostic, the embedding neighborhood should be such that it can represent any underlying model’s

Algorithm 1: Training the GIN model \mathcal{M}_G

Require: Number of epochs N_e , hyperparameters h_{RW} (See App. G) for the Random Walker

Ensure: Learn parameter set Θ_G

- 1: **for** epoch $i \leftarrow 1$ to N_e **do**
 - 2: $W_p \leftarrow$ Sample a batch of positive random walks with h_{RW}
 - 3: $W_n \leftarrow$ Sample a batch negative random walks by selecting a set of random nodes
 - 4: Back-propagate the average loss (Equation 16) using \mathcal{M}_G on W_p and W_n
 - 5: **return** Θ_G
-

representation. GIN has been shown to be a maximally powerful GNN model. In particular, it has been shown to be as powerful as a *Weisfeiler-Lehman (WL) graph isomorphism test*, which assigns canonical labels such that unique labels guarantee that the two graphs are not isomorphic. (Xu et al. 2019b) shows that injectivity of the neighborhood aggregation function is a necessary condition for a GNN to simulate a WL test and give one such example in GIN. Hence, any underlying black-box GNN model has less representation power by aggregating information from their neighbors than a GIN. This motivates us to use a GIN to model the neighborhood for distortion, so that we can effectively attack any target black-box model.

In order to further justify our claim, we conduct an ablation study and compare the performance of our attacks using a GCN and a GIN as our embedding model. Both are trained in the same unsupervised manner. Figure 5 compares the $DA(\%)$ across different budgets when using GCN embeddings as compared to when using GIN embeddings for node classification in CoRA dataset. The results are interesting and show the apparent trade-off in using a theoretically powerful GIN model to attack common GNN target models. While GCN embeddings are able to transfer the neighborhood better (our method produces more DA, higher is better) for GNNs that are based on *neighborhood convolution*, they do not get transferred well to the *locality-aware P-GNN* (Figure 5e).

Hence, this shows that our strategy can be tuned based on the amount of information that is made available to the attacker. In a completely model-agnostic setting, it is reasonable to use a powerful GIN model to generate embeddings. If we know some distinct features about the underlying model, then it will be more beneficial to use an embedding model that has a similar or most representative neighborhood aggregation function, so that the knowledge of neighborhood distortion gets transferred well.

Furthermore, it is worthwhile to note here that if the attacker wishes to leverage the task-agnosticism, then they might even use an embedding model trained for that specific task (in which case, the embeddings/representations would be specially tuned to the attack scenario). TANDIS is a generic and unique framework that allows this kind of tuning according to the available attack/model information.

D Rationale behind two GNNs

The GNNs serve different roles. The role of μ_v is to effectively characterize the state-space (Eq. 11) and actions (Eq. 12), and capture the combinatorial nature of the problem. Hence, the GCN embeddings μ_v are trained end-to-end in the DQN along with an MLP to learn the Q -function. On the other hand, GIN embeddings \mathbf{Z}_v are trained independently to characterize neighborhood distortion. Furthermore, while the GIN is trained in a transductive manner with one-hot encodings of nodes, the GCN trains in an inductive manner, where in the initial layer the nodes are characterized by their feature vectors \mathcal{X}_v (Recall § 2).

E Greedy Selection of Edge Perturbations for Training

Algorithm 2 describes how the Q -function is learned in the RL setup (Section 3.4) of TANDIS. In particular, for each node in the training set, we generate perturbations for T steps following a ϵ -greedy strategy, as noted in Step 4 (Algorithm 2). Each such perturbation can be represented by a tuple storing the current state, new state, action, and accumulated rewards (defined in Section 3.4). This is stored in an “experience replay” memory, from which a batch of samples is randomly sampled. Finally, this batch is used to backpropagate the squared loss. We repeat this process for L steps.

Algorithm 2: Learning Q -function

Require: Trained GIN model \mathcal{M} , hyper-parameters M, N relayed to fitted Q -learning, number of episodes L and sample size T .

Ensure: Learn parameter set Θ_Q

- 1: Initialize experience replay memory M to capacity N
 - 2: **for** episode $e \leftarrow 1$ to L **do**
 - 3: **for** step $j \leftarrow 1$ to T **do**
 - 4: $v_j \leftarrow \begin{cases} \text{random node } v \notin S_j; \text{ with probability} \\ \epsilon = \max\{0.05, 0.9^j\} \\ \text{argmax}_{v \notin S_j} Q'_n(S_j, v; \Theta_Q); \text{ otherwise} \end{cases}$
 - 5: $S_{j+1} \leftarrow S_j \cup \{v_j\}$
 - 6: **if** $t \geq n$ **then**
 - 7: Add tuple $(S_{j-n}, v_{j-n}, \sum_{i=j-n}^t r(S_i, v_i), S_j)$ to M
 - 8: Sample random batch B from M
 - 9: Update Θ_Q by Adam optimizer for B
 - 10: **return** Θ_Q
-

F Complexity Analysis

Train phase The training complexity consists of two parts – (1) Training the GIN, and (2) Training the DQN. GIN is trained in an unsupervised manner, following Algorithm 1. This accounts for a training complexity of $O(N_e l h_g T_r)$, where N_e is the no. of epochs, l is the no. of GIN layers, h_g is the hidden dimension of GIN, and T_r is the time for random walk generation. We follow node2vec’s code (Grover and Leskovec 2016) to generate random walk,

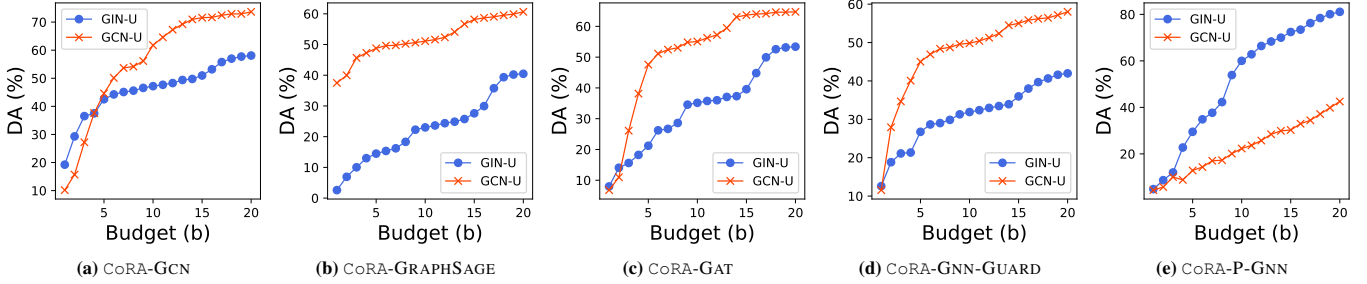


Figure 5: **Ablation study: Comparison of using GCN v/s GIN embeddings for distortion in the TANDIS attack for the node classification task in CoRA.** GIN-U represents that GIN is trained in an unsupervised manner.

which accounts for $O(L_r/(k_r(L_r - k_r)))$, where L_r is the length of the random walks, k_r is the no. of samples to generate. The second part in the analysis is due to DQN, which is trained by following Algorithm 2. This accounts for $O(LT|\mathcal{V}|(Bh_m h_{gc} + (|\mathcal{E}|h_{gc} + |\mathcal{V}|h_{gc}^2)))$, where L is the no. of episodes, T no. of time steps, B batch size, $|\mathcal{V}|$ no. of nodes, $|\mathcal{E}|$ no. of edges, h_m dimension of MLP, and h_{gc} dimension of GCN layers respectively. $h_m h_{gc}$ is the time for MLP forward pass, and $(|\mathcal{E}|h_{gc} + |\mathcal{V}|h_{gc}^2)$ is the time for GCN forward pass (as derived in the next section).

Test phase To find $Q'_n(S_i, e)$, we do a forward pass on a k -layer GCN followed by an L -layer MLP. We ignore the factors of k and L as their values are usually small and fixed (≤ 3), and assume the average degree in \mathcal{G} to be d .

GCN: We assume the hidden dimension to be h_g . Each node draws messages from their neighbors and performs a mean pool, followed by linear transformation through weight matrices \mathbf{W}_{GCN}^l . These operations consume $O(d \cdot h_g)$ and $O(h_g^2)$ respectively. When performed over all nodes in \mathcal{G} , the complexity is $O(|\mathcal{E}|h_g + |\mathcal{V}|h_g^2)$.

MLP: The transformations performed by the MLP is outlined in Eq. 14. The representation dimensionality of a state and an action are h_g (Eq. 11) and $2h_g$ (Eq. 12) respectively. If the hidden dimension in the MLP is h_m , then computing μ_{s_i, a_i} in Eq. 14 consumes $O(h_g \cdot h_m)$. The final conversion to a scalar (predicted long-term rewards) consumes an additional $O(h_m)$ cost. This operation is repeated over each candidate edge since we choose the one with the highest predicted reward. Hence, the total complexity is $O(|\mathcal{V}|(h_m(1 + h_g)))$.

Combining the costs from both GCN and MLP, and the fact that we make \mathcal{B} forward passes, the total computation complexity is $O(\mathcal{B}(|\mathcal{E}|h_g + |\mathcal{V}|h_g^2 + |\mathcal{V}|(h_m(1 + h_g))))$. Since h_g and h_m are fixed constants, the complexity with respect to the input parameters reduces to $O(\mathcal{B}(|\mathcal{E}| + |\mathcal{V}|))$.

G Experimental Setup

All experiments are performed on a machine running Intel Xeon G-6148 with a setting of 20 cores of 2.4 GHz, one Nvidia V100 card with 32 GB GPU memory and 192 GB RAM with Ubuntu 16.04.

Datasets	# Nodes	# Edges	# Node Labels
Cora	2.7K	5.4K	7
Citeseer	3.3K	4.7K	6
PubMed	19K	44K	3

Table 5: **Datasets used in the experiments.**

Datasets We use three real-world datasets in our experiments following (Chang et al. 2020): CoRA (McCallum et al. 2000), CiteSeer and PubMed (Sen et al. 2008). These are citation networks where vertices denote documents with bag-of-words features and edges denote citation links. We consider only the largest connected component which is consistent with our baseline setup (Chang et al. 2020). The statistics of the datasets are shown in the Table 5.

Tasks

Node Classification: All the target models are trained for the node classification task using 10% of the nodes each for training and validation. The remaining 80% nodes are used for the testing where each node is separately considered as a target node for the attack strategies and the average accuracy quantified as $DA(\%)$ in Equation 15. For the large dataset Pubmed, we consider a randomly sampled 10% of the nodes out of the test set and we present the average value after 5 different runs.

Link Prediction: All the target models are trained using a binary cross entropy loss for this task using 10% of the positive and negative links each for training and validation. Note that we ensure down-sampling of the majority class and thus, ensure that equal number of positive (existing) and negative (non-existing) links are considered in our training, validation and test sets. We consider a randomly sampled 30% links for the test set and note the average drop in accuracy after considering each links separately. Each target link is attacked by considering one of the end-nodes as the target node on which edges can be added or deleted. We randomly sample 10% of the test set for the large dataset Pubmed and note the average value after five different runs.

Pairwise node-classification: The setup is similar to the task of link prediction except for the end-labels which de-

note the equality of node pairs’ labels rather than an existence of an edge between them. Thus, the class distribution is now balanced based on this label. We follow a 10–10–30 split here as well and take 10% sample to target Pubmed.

Parameters Our framework (Figure 1) needs two trainable models, GIN and DQN. These are trained separately and have different hyper-parameters as described below.

GIN: We use a 2-layer GIN model with hidden dimension of 16. Here also, we use 10% each for training and validation. This is trained in an unsupervised manner. To generate the random walks, we use $p = q = 1$ (where p and q denote the likelihood of return and measure of in-out search respectively (Grover and Leskovec 2016)), a walk length of 20, a context size of 10 and do 10 walks per node.

DQN: To train the DQN component, we use Deep Q-learning as noted in the Algorithm 2. Here, the number of episodes L and number of steps T are fixed to be 100 and 10 respectively. Also, n is fixed to be equal to 2 and thus, we consider a 2-step Q-function. To model the DQN, we consider a 2-layer GCN followed by a 2-layer MLP, both with hidden dimensions of 16. We use 40% nodes as targets for the training the DQN out of which the replay memory is made, following ϵ -greedy steps.

Baselines

RL-S2V: We use the RL-S2V (Dai et al. 2018) in a model-agnostic manner following the formulation mentioned in GF-ATTACK (Wang et al. 2020). In particular, we train the Deep Q-network using a surrogate GCN model and then transfer these attacks to all our target models (as mentioned in Section 4). Also, note that the surrogate GCN is trained differently than the target GCN model. We train for 100000 steps for each dataset and separately for each budget (until 5 as noted in Table 2).

GF-ATTACK (Wang et al. 2020): This is the state-of-the-art in the restricted black-box setting and the only available task-agnostic attack framework. It attacks the embeddings by perturbing the corresponding graph filters. While the exact optimization may depend upon the type of black-box model to attack, we can exploit the transferability of these attacks and make it model-agnostic. We use the GCN setting mentioned in (Wang et al. 2020) to attack each of our black-box models. For link tasks, we use the same strategy as ours and target a randomly chosen end-node.

H Additional Results

Non-neural Baselines Here, we compare our method TANDIS against two non-neural baselines — RANDOM and DEGREE, as defined in (Chang et al. 2020). Figure 6 shows the results of these baselines for node classification task in CoRA and CiteSeer compared with TANDIS. Note that our method comprehensively outperforms these baselines.

Comparison with Greedy Figure 7 shows the comparison between our proposed RL optimization of Equation 10 (i.e., TANDIS) and the corresponding greedy optimization (i.e., Greedy) for 10 targets on the node classification task

in CoRA and CiteSeer. While Greedy does consistently better, the time taken is more than 4 orders in magnitude (See Fig. 7(d) and Fig. 7(h)). Thus, even though we can obtain better performance by greedily optimizing the proposed neighborhood distortion, the trade-off for efficiency is huge, which makes the proposed RL optimization more scalable and efficient for finding optimal perturbations maximizing neighborhood distortion (i.e., Equation 9).

Interpretability In this section, we study additional node properties in order to interpret the neighborhood distortion. In order to do that, we choose the following different node-level properties.

Feature and Graph Properties

- **Feature Similarity:** Jaccard similarity of node features of the target and the candidate node for perturbation.
- **Degree:** In an undirected graph, the node degree is the number of edges adjacent to the node. In a directed graph, the in-degree and the out-degree of a node is the number of edges incident on the node, and the number of outgoing edges from the node respectively. In our case, since we have conducted our study on undirected graphs, the first definition holds true. However, a similar study can easily be conducted in case of a directed graph.
- **Local Clustering Coefficient:** The local clustering coefficient of a vertex is given by the ratio of the actual number of links between the vertices in its neighborhood divided and the total no. of possible links that can exist between these neighbor vertices.
- **Reverse k -NN Rank:** Position of the candidate node in the ranked list of nodes, sorted in descending order, according to the number of times the node occurs in the 2-hop neighbourhood of all the other nodes in the graph.

Community Based Properties We have also taken into consideration a few community related measures. For a given target t we define its community, S , as the 50 nearest neighbours in the original embedding space. Considering the fact that upon perturbation, the neighbourhood of the target becomes distorted, we define the perturbed community, S' , of target t as the 50 nearest neighbours in the perturbed embedding space. We expect that after perturbation, the quality of the community should worsen. Throughout the definitions stated further, $m(S)$ denotes the number of edges between the nodes in community S , and $c(S)$ denotes the number of edges between nodes in S and the rest of the network, i.e., nodes in $\mathcal{V} \setminus S$. $c(S)$ is also known as cut size of S .

- **Edge Expansion Difference (ΔEE):** The edge expansion (EE) is defined as the ratio of cut size and minimum of the cardinalities of the two communities S and $\mathcal{V} \setminus S$. We consider the edge expansion difference (ΔEE) as:

$$\Delta EE = EE(S, \mathcal{V}) - EE(S', \mathcal{V}) \quad (17)$$

where,

$$EE(S, \mathcal{V}) = \frac{c(S)}{\min(|S|, |\mathcal{V} \setminus S|)} \quad (18)$$

denotes the edge expansion of the community S .

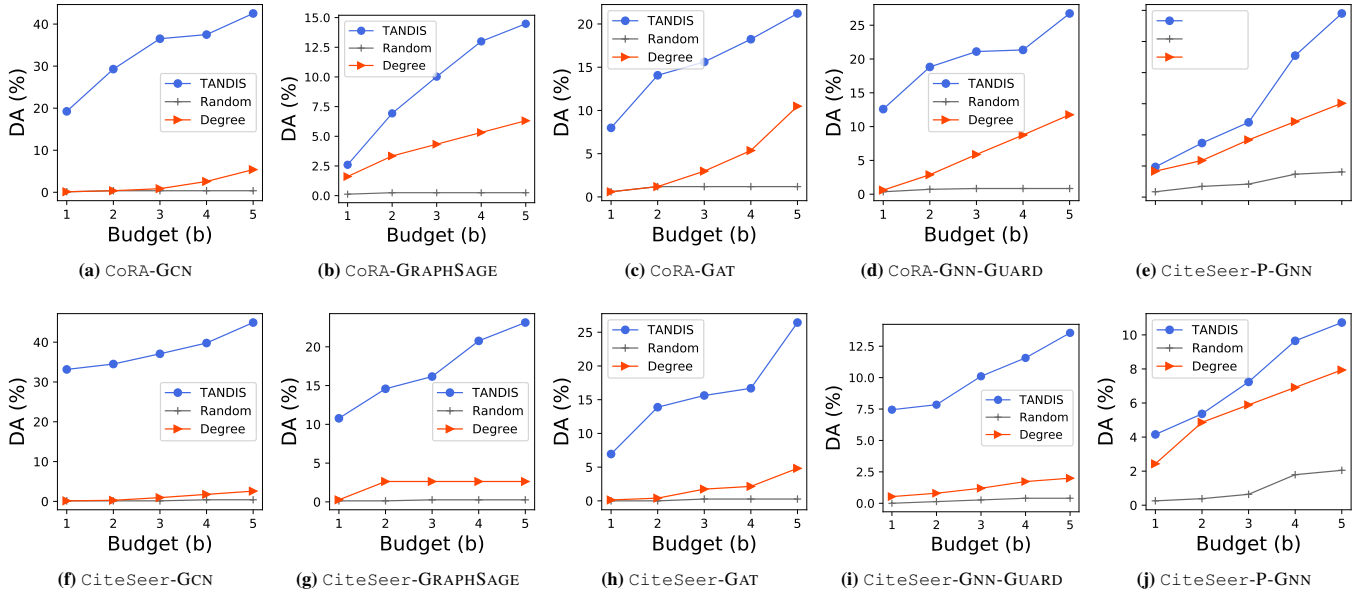


Figure 6: Comparison of non-neural baselines with TANDIS for the node classification task in CoRA and CiteSeer. TANDIS outperforms the baselines in all cases.

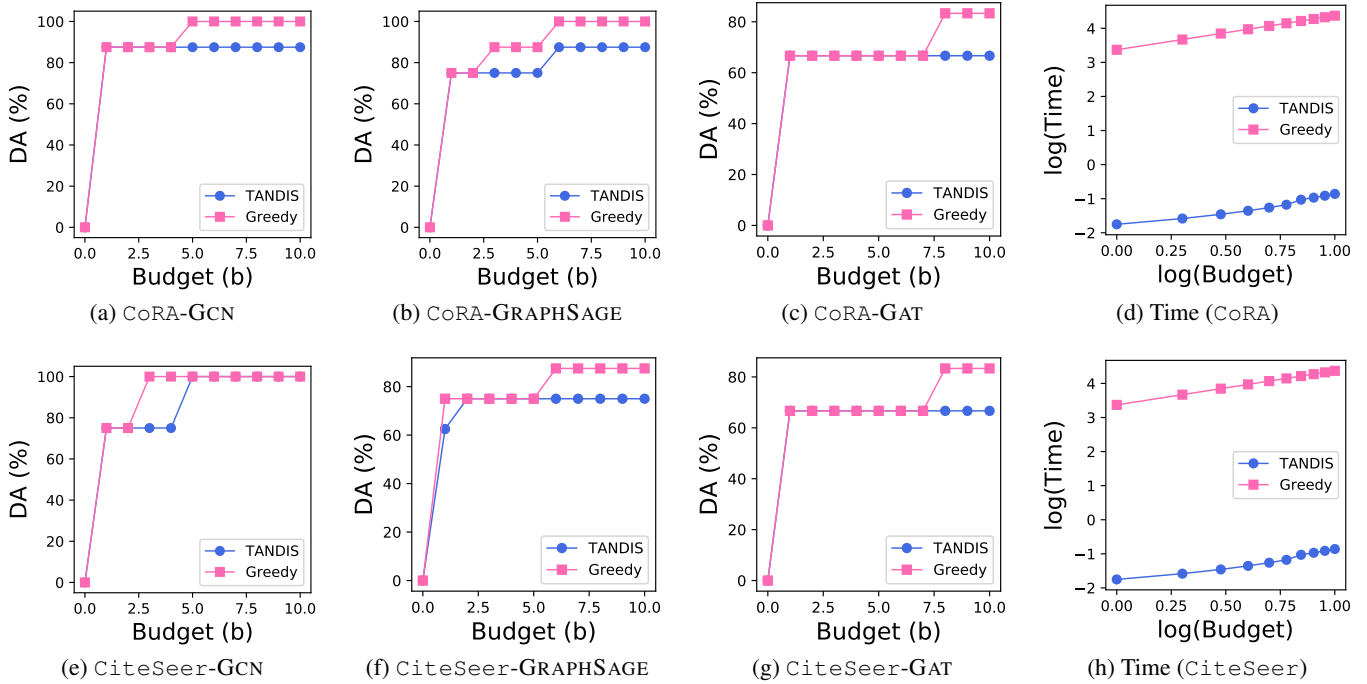


Figure 7: Comparison of TANDIS with its non-neural Greedy equivalent for the node classification task in CoRA and CiteSeer averaged over 10 targets. Greedy performs better than TANDIS, but it takes time more than 4 orders of magnitude with an improvement of only $\sim 20\%$. So, Greedy is not practically feasible.

Property	Correlation	p -value
Feature similarity	-0.20 ± 0.196	< 0.001
Degree	-0.15 ± 0.008	< 0.001
Local Clustering Coefficient	0.25 ± 0.004	< 0.001
Reverse k-NN rank	0.02 ± 0.008	0.37
Edge Expansion Difference	0.03 ± 0.014	0.24
Conductance Difference	0.01 ± 0.010	0.65
Normalized-Cut Size Difference	0.01 ± 0.010	0.67
Volume Difference	0.02 ± 0.017	0.37

Table 6: Spearman’s Rank Correlation of various node properties with neighborhood distortion along with their statistical significance.

- **Conductance Difference (ΔC):** Conductance ($C(S)$) is the fraction of edge volume that points outside the community S , where edge volume is defined as the sum of node degrees of the nodes in the community. We consider the conductance difference (ΔC) as a property:

$$\Delta C = C(S) - C(S') \quad (19)$$

where,

$$C(S) = \frac{c(S)}{(2m(S) + c(S))} \quad (20)$$

denotes the conductance of the community S .

- **Volume Difference (ΔV):** The volume ($V(S)$) of a community S , is the sum of (out-)degrees of the nodes in S in case the graph is directed, or only the sum of degrees of the nodes in S , if the graph is undirected. For our case the latter holds. We consider the volume difference (ΔV) as a property:

$$\Delta V = V(S) - V(S') \quad (21)$$

where,

$$V(S) = (2m(S) + c(S)), \quad (22)$$

denotes the volume of the community S .

- **Normalized Cut Size Difference:** The normalized cut size is the cut size multiplied with the reciprocal of the volumes of the two sets S and $\mathcal{V} \setminus S$. We consider the normalized cut size difference (ΔNCS) as a property:

$$\Delta NCS = NCS(S, \mathcal{V}) - NCS(S', \mathcal{V}) \quad (23)$$

where,

$$NCS(S, \mathcal{V}) = c(S) \left(\frac{1}{2m(S) + c(S)} + \frac{1}{2(|\mathcal{E}| + m(S)) - c(S)} \right), \quad (24)$$

denotes the normalized cut size of the community S .

Table 6 shows the Spearman’s Rank Correlation of these properties with the neighborhood distortion measure. As we have already seen in Section 4.4, only **Degree**, **Feature Similarity**, and **Local Clustering Coefficient** show significant correlations and the possible reasons for them. Now, it is important to note that the lack of significance in the correlation with the community-based metrics indicates that the neighborhood distortion may not necessarily bring a difference in the local community around the target node, as defined by

these community based measures. In particular, the perturbation is not large enough to cause a significant change in the entire neighborhood community but only enough to cause a change in the inference for the downstream task. Additionally, the low magnitude of significant correlation with the three parameters (i.e., degree, feature similarity, and local clustering coefficient) further strengthens the claim that the distortion is difficult to detect with standard attack detection techniques (Sun et al. 2018).

I Reproducibility and Code-base

The code is made available at <https://github.com/idea-iitd/TANDIS>.